RESEARCH

Tunable Magnetic Skyrmion Motion on a Nanostrip Using Current and Spin Waves: A Micromagnetic Study

Payal Bhattacharjee[1] · Saswati Barman[1,2]

© The Author(s), under exclusive licence to Springer Science+Business Media, LLC, part of Springer Nature 2024

Abstract

Nowadays, the concept of non-trivial topological protection and the nanoscale size of nanomagnetic particles constitute a major area of research. Due to topological protection stability, nanoscale size, and the requirement of low spin current density for motion, skyrmions have attracted great attention in next-generation spintronic devices as robust information carriers. We study the motion of an isolated magnetic skyrmion with induced interfacial Dzyaloshinskii-Moriya interaction (iDMI) instigated by spin waves and driven by spin current with variation in different parameters in a nanotrack of finite length using micromagnetic simulations. It is found that the magnetic skyrmion moves in the same direction as the direction of propagation of the spin waves. The skyrmion initially experiences an acceleration in its motion; thereafter, the velocity decreases exponentially. The motion of the magnetic skyrmion initiates as the momentum of the spin wave gets transferred to it. The motion of the magnetic skyrmion is found to be significantly dependent on the variation of parameters like frequency and amplitude of the incident spin waves, as well as the damping parameter and the strength of the applied spin-polarized current. The results obtained in this work could become useful to design skyrmion-based spintronic information-carrying and storage devices.

1 Introduction

To overcome the drawback of increasing leakage power in on-chip memories arising from CMOS technology, the requirement of non-volatile memory technologies enabling low power dissipation has been proposed [1]. At the burning juncture, the nanomagnetic element-based non-volatile memories and technologies have earned a huge promising candidature in this consideration. One of the most predicted non-volatile data storage devices is the racetrack memory (RM), which was basically proposed to make use of domain walls as carriers in information-carrying devices [2–4].

These racetrack memories have low power consumption and faster accessible times as compared to present-day random access memories (RAM) and hard disk drives (HDD) [3]. But in addition to the spintronic-based devices, the concept of topology has gathered extensive research interest in the scientific community at large. Due to the topological protection, the most predominant nanomagnetic specimen in this regard is the magnetic skyrmion [5]. The small size and the topology of magnetic skyrmion make it an encouraging aspirant as an information carrier in the design of data storage devices in the near future [6, 7]. Thus, complete control of the skyrmion motion is of the utmost necessity.

Coined initially by the British nuclear physicist Tony Skyrme in the context of the field-theoretical description of interacting pions, skyrmions were proposed in the 1960s [8, 9]. These two-dimensional magnetic skyrmions have chiral spin textures and can be stabilized in various types of materials, which include ultrathin films [10–13], non-centrosymmetric bulk magnets [14–16], and nanowires [17, 18]. In a ferromagnetic medium, the magnetic skyrmions have a continuous changing magnetization density, whereas

---

✉ Saswati Barman
Saswati.Barman@iem.edu.in

1 Department of Basic Sciences and Humanities, Institute of Engineering & Management, Salt Lake Electronics Complex, Sector V, Salt Lake, Kolkata 700091, India

2 University of Engineering & Management, University Area, Plot No. III, B/5, New Town Road, Action Area III, Newtown, Kolkata 700160, India

the center is oriented in the opposite direction from its surroundings. This topological spin structure is due to the competition between the exchange energy, which favors the parallel alignment of neighboring spins, and the chiral interaction known as the Dzyaloshinskii-Moriya interaction (DMI), which prefers the orthogonal alignment of the spins [19–21]. These interactions mainly arise due to the lack of inversion symmetry at the interface of magnetic films or in the lattices. For two neighboring spins S_1 and S_2, the DMI between them is given by $H_{DM} = -D_{12} \cdot (S_1 \times S_2)$, where D_{12} is the DMI strength. The interfacial DMI in magnetic thin films between two neighboring spins has been speculated to result from an indirect exchange mechanism between them and a neighboring atom with a large spin-orbit coupling (SOC) [22, 23].

Magnetic skyrmions, especially Néel skyrmions, can be created in ultrathin ferromagnet or heavy metal films, which have a vast application in spintronics [24]. These topological nanomagnetic structures have proved to be a potential candidate for information carrier devices due to their ultra-high data storage density and negligible joule heating [17, 25, 26]. Skyrmion-based racetrack memory (RM) has captivated wide attention for next-generation spintronic devices due to their small size and the extensively negligible energy required for their motion [27, 28]. An isolated skyrmion can be created by various means, such as spin current, pulse current, in-plane current, electric field, and magnetic field [29–32]. The skyrmion motion can be driven and controlled by the application of spin-polarized current as well as spin waves [33–35].

In this paper, we investigated the motion of an isolated skyrmion with DMI in a nanostrip with perpendicular magnetic anisotropy using micromagnetic simulations. We apply spin wave and spin-polarized current to the nanostrip, which causes the skyrmion to move along the direction of spin wave propagation. This motion of the magnetic skyrmion is due to the spin-transfer mechanism and follows the same spin-conservation rules as domain walls. We systematically investigate the motion of the skyrmion along the nanostrip with the variation in amplitude and frequency of the applied spin wave, the current density of the spin-polarized current, and the

Gilbert damping parameter. We find that the skyrmion velocity differs significantly under variations in different parameters, but the spin texture of the skyrmion does not change throughout the motion across the nanotrack with these variations in the parameters. Our findings indicate that an isolated magnetic skyrmion can be driven

effectively by the application of spin waves and a spin current, and their velocity is largely dependent on the amplitude and frequency of the incident spin waves as well as the applied spin-polarized current density and the Gilbert damping parameter of the material. The magnetic skyrmion on a nanostrip proves to be one of the most promising candidates from a technological perspective and definitely proposes a new path to design and develop an effective skyrmion racetrack memory.

2 Methods

2.1 Theory and Micromagnetic Simulation Details

To study the dynamics of the nanomagnets, micromagnetic simulation has always been a dominant method. We here perform the micromagnetic simulations using Object-Oriented Micromagnetic Framework (OOMMF) with the inclusion of DMI module [36]. When a current is applied, the resulting spin dynamics of magnetization is controlled by the Landau–Lifshitz–Gilbert (LLG) equation including the Slonczewski-like spin-transfer torque which is a damping-like torque [37–40]:

$$\frac{dm}{dt} = -|\gamma_o| \left[m \times H_{eff} + \alpha \left(m \times \frac{dm}{dt} \right) - \frac{\gamma_o \hbar jP}{2\mu_o ebM_s} [m \times (m \times p)] \right] \tag{1}$$

where $m = \frac{M}{M_s}$, M is the magnetization, M_s is the saturation magnetization, H_{eff} is the effective field, γ_o is the Gilbert gyromagnetic ratio, b is the thickness of the nanotrack, P is the spin polarization, p is the (unit) electron polarization direction, α is the Gilbert damping parameter, j is the current density, and $\hbar$ and e being the reduced Planck's constant and electronic charge respectively. The effective field can be defined as:

$$H_{eff} = \mu_o^{-1} \frac{\partial E}{\partial M} \tag{2}$$

where μ_o is the permeability of the free space, E is the average energy density which is a functional of M and is given by [6, 37, 41]:

$$E = A[\nabla \left(\frac{M}{M_s} \right)]^2 - K \frac{(n.M)^2}{M_s^2} - \mu_o M.H - \frac{\mu_o}{2} M.H_d(M) + \frac{D}{M_s^2} \left(M_z \frac{\partial M_x}{\partial x} - M_x \frac{\partial M_z}{\partial x} + M_z \frac{\partial M_y}{\partial y} - M_y \frac{\partial M_z}{\partial x} \right) \tag{3}$$

where A is the exchange energy constant, K is the anisotropy energy constant; H and H_d are the applied and self-interaction field, D is the DMI constant while M_x, M_y, and M_z are the components of magnetization.

We investigate the motion of an isolated magnetic skyrmion in a finite FM monolayer nanotrack (nanostrip)

Fig. 1 **a** Schematic of the CIP geometry. **b** Initial stable state of an isolated skyrmion on a magnetic nanostrip. The image at the inset shows the spatial distribution of spin texture of the Neél skyrmion. The z-component of the magnetization is given by the background colour (orange: positive and green: negative). The colour bar indicates the out of plane magnetization component m_z which has been used throughout the paper. The coordinate axes are shown adjacent
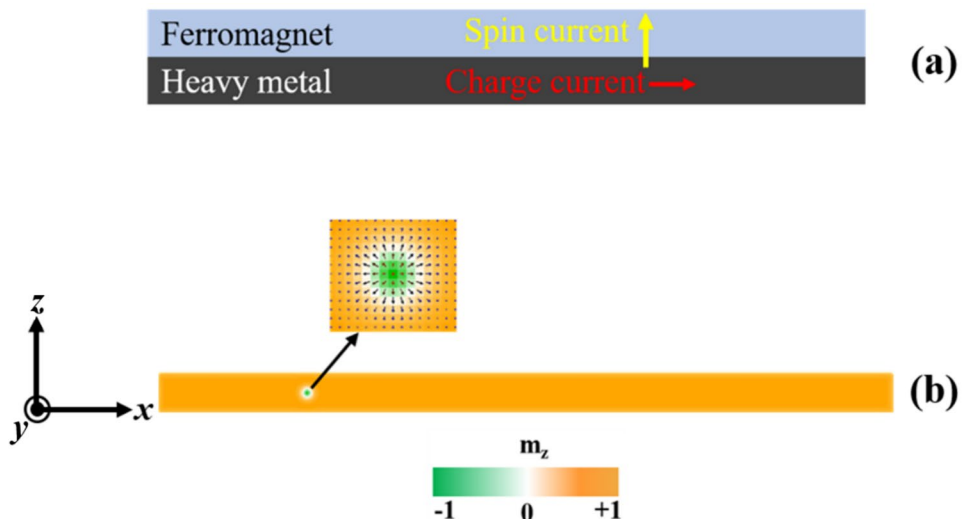
with perpendicular magnetic anisotropy (PMA) and interfacial Dzyaloshinskii-Moriya interaction (iDMI) and present the report of the resulting trajectory of the skyrmion along the nanostrip. We investigate the current and spin waves driven magnetic skyrmion velocity induced by the 'vertical' spin current in the nanostrip with CIP geometry (Fig. 1a). For micromagnetic simulations, we consider a finite nanostrip of length one micron along the x-axis, width 100 nm in the y-direction and thickness 1 nm along the z-direction. The nanostrip was discretized into cells having cell size $2 \times 2 \times 1$ nm^3 respectively for simulation. The parameters used in the simulation are similar to that are compatible to Co/Pt layers: [6] DMI constant $D = 3.5 \times 10^{-3} \, J/m^2$, saturation magnetization $M_s = 580 \times 10^3 \, J/m$, exchange stiffness constant $A = 1.5 \times 10^{-11} \, J/m$, perpendicular magnetic anisotropy $K = 0.8 \times 10^6 \, J/m^3$, and $= \gamma_o = -2.21 \times 10^5 \, m/A.s$. Initially, to create a magnetic skyrmion, we have injected a vertical spin current having current density $j = 1.2 \times 10^{14} \, A/m^2$ along negative z-axis for a very short period of time ($t = 0.3 \, ns$) at $x = 200 \, nm$ from the left edge of the nanostrip. Then, we relax the system for $20 \, ns$ to get the stable state. The Gilbert damping parameter is kept at $\alpha = 0.3$ during the creation of the skyrmion using spin current. The maiden stable state of the Neél-type magnetic skyrmion is shown in Fig. 1b. To study the mobility of the magnetic skyrmion along the nanostrip, we apply a spin-polarized current and injected a spin wave along with it. The parameters used in the simulations are kept the same as before with the exception in the Gilbert damping parameter ($\alpha = 0.01$). The simulations are executed for a time duration of $40 \, ns$.

3 Results and Discussion

3.1 Skyrmion on a Nanostrip

To study the dynamics of the isolated skyrmion, we applied a spin-polarized current with a relatively small value of current density ($j = 8 \times 10^{10} \, A/m^2$) and a degree of polarization $p = 0.4$. In the CIP geometry, the heavy metal substrate is directly injected with a charge current that flows in the right direction (positive x-direction), while the equivalent electrons flow in the left direction. The charge current will change into a spin current that travels perpendicularly to the FM nanotrack because of the SHE in the heavy metal. Hence, the spin current generates the STT effect, which may be responsible for the skyrmion motion, by exerting a global force on the magnetic spins in the FM nanotrack. We have also injected the spin wave simultaneously with the spin-polarized current by applying a sinusoidal magnetic field of the form $\boldsymbol{H} = H_o \sin(2\pi ft)\widehat{y}$ at a small patch of the nanostrip along the positive y-axis, where H_o is the amplitude of the magnetic field and f is the frequency. The location of the ac magnetic field ($x = 0$ to $50 \, nm$) is offset from that of the magnetic skyrmion. The majority of the spin waves propagate in the x direction. The excited spin waves have the same frequency as the alternating current magnetic field. The spin waves, however, will be reflected as it travels to the end of the strip. To avert the reflection of spin waves from the extreme right end of the nanostrip, we set $\alpha = 1$ at $x \geq 850 \, nm$. The excited spin wave propagates along the nanotrack and pushes the skyrmion along the nanotrack. This is due to the interaction between the incident spin wave and the skyrmion, which

Fig. 2 **a** Formation of domain walls at frequencies $f = 60\,GHz$, $140\,GHz$; **b** the location of the skyrmion (velocity is slowed down) at $f = 190\,GHz$. All the snapshots have been taken at time $t = 40\,ns$

exerts a torque on the skyrmion compelling it to move. We look into the trajectory of the magnetic skyrmion along the nanostrip with the variation in the frequency and amplitude of the applied radio-frequency field (spin wave), Gilbert damping parameter, and spin-polarized current density.

3.1.1 Variation of the Frequency of the Spin Wave

We vary the frequency of the applied spin wave from $10\,GHz$ to $200\,GHz$ and track the motion of the skyrmion along the nanostrip. The amplitude of the spin wave is kept at $500\,mT$, and the Gilbert damping parameter at $\alpha = 0.01$. At very low frequencies (up to $20\,GHz$), the skyrmion traverses the nanostrip, but it follows a zigzag path along its motion. The lateral width constriction of the ferromagnetic nanotrack creates a potential barrier, which prevents the magnetic skyrmion from being smoothly directed along the nanotrack for frequencies

of spin waves less than $20\,GHz$. From frequencies equal to $30\,GHz$ up to $170\,GHz$, the skyrmion decays with the formation of a domain wall a few nanoseconds after the start of its motion. The motion of the skyrmion along the nanostrip is observed from $f = 175\,GHz$. From $190\,GHz$ onwards, the skyrmion velocity slows down. This finding led to the choice to drive the skyrmion at a frequency of $180\,GHz$ in the next simulations. Figure 2a shows the formation of domain walls at frequencies $60\,GHz$ and $140\,GHz$, while the motion of the skyrmion along the nanostrip at $190\,GHz$ at $t = 40\,ns$ is shown in Fig. 2b. Figure 3a shows the instantaneous velocity of the skyrmion motion in the frequency range $177 - 185\,GHz$ in $40\,ns$ time duration. The skyrmion is initially at rest, but it starts moving with acceleration as the spin wave reaches the position of the skyrmion. It moves with an acceleration and suffers a deceleration after reaching the maximum velocity. This is due to the fact that, as the amplitude of the excited spin wave decreases as it moves away from the point of excitation, it decays gradually, and the velocity of the skyrmion decreases [Supplementary Information; Fig. S1]. But it continues to move due to the spin current. Theoretical studies have illustrated that the motion of a magnetic skyrmion is due to the transfer of momenta between the skyrmion and the spin waves, and it is mainly driven by the scattering of magnons [42]. At frequencies $f = 177\,GHz$ and $f = 179\,GHz$,

Fig. 3 Instantaneous velocity of the magnetic skyrmion when the following parameters are varied: **a** frequency of the spin wave, **b** amplitude of the spin wave, **c** Gilbert damping parameter, and **d** current density strength
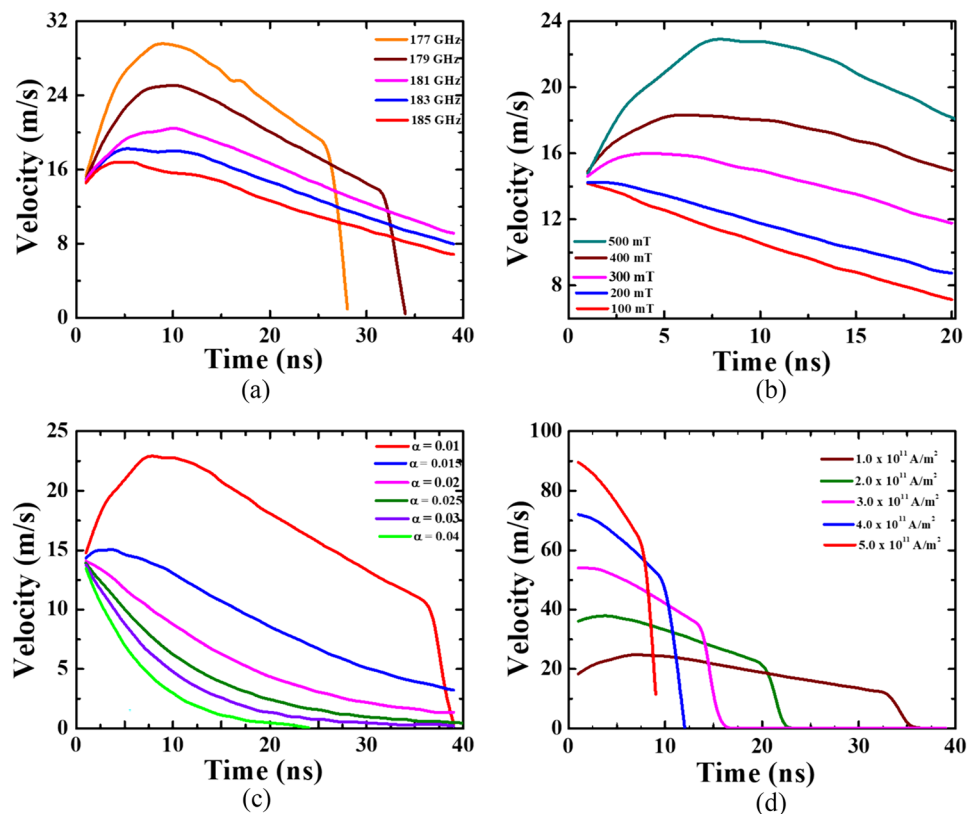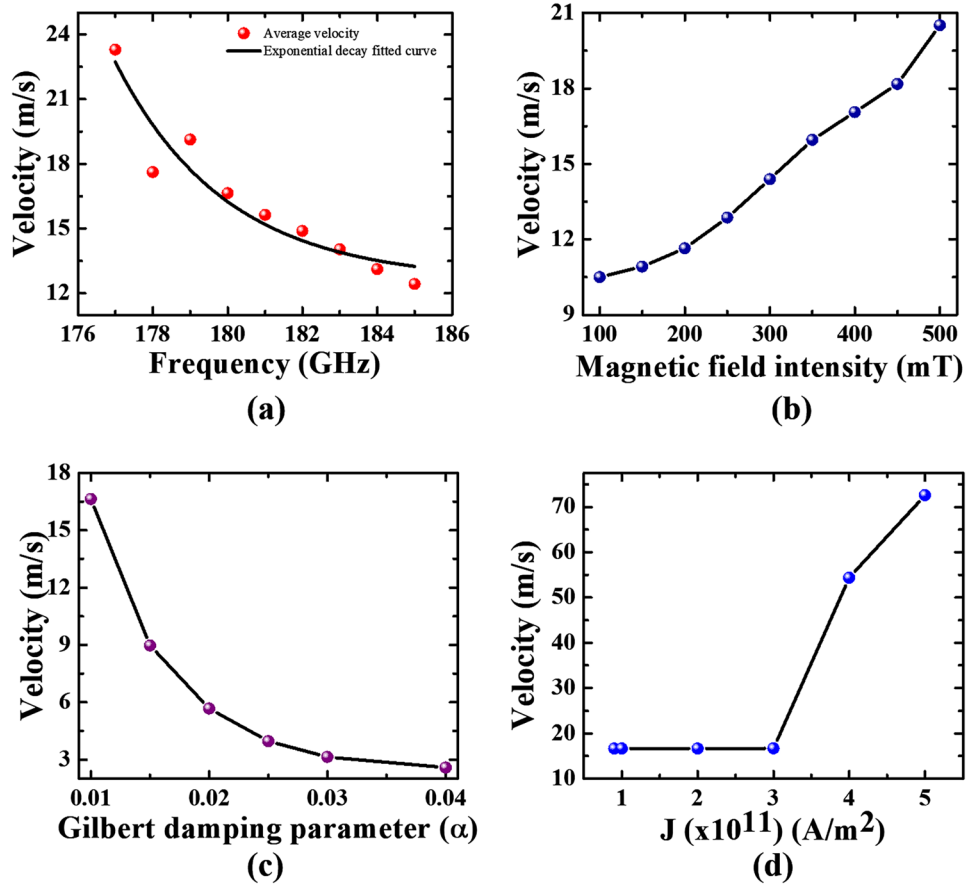
Fig. 4 Average velocities of the skyrmion as it moves along the nanotrack at different parameters: **a** frequency of the spin wave, **b** amplitude of the spin wave, **c** Gilbert damping parameter, and **d** current density strength

the magnetic skyrmion acquires a large acceleration in the initial stage of movement and has a higher velocity; thereafter, the velocity decreases gradually. At higher frequencies equal to $183\,GHz$ and $185\,GHz$, the skyrmion experiences negligible acceleration during its movement along the track. At a frequency equal to $178\,GHz$, the skyrmion moves 483 nm at $t = 20\,ns$, while it moves 410 nm at $f = 180\,GHz$ at $t = 20\,ns$. Figure 4a shows the average velocity of the magnetic skyrmion at different applied frequencies. Figure 5a displays the position
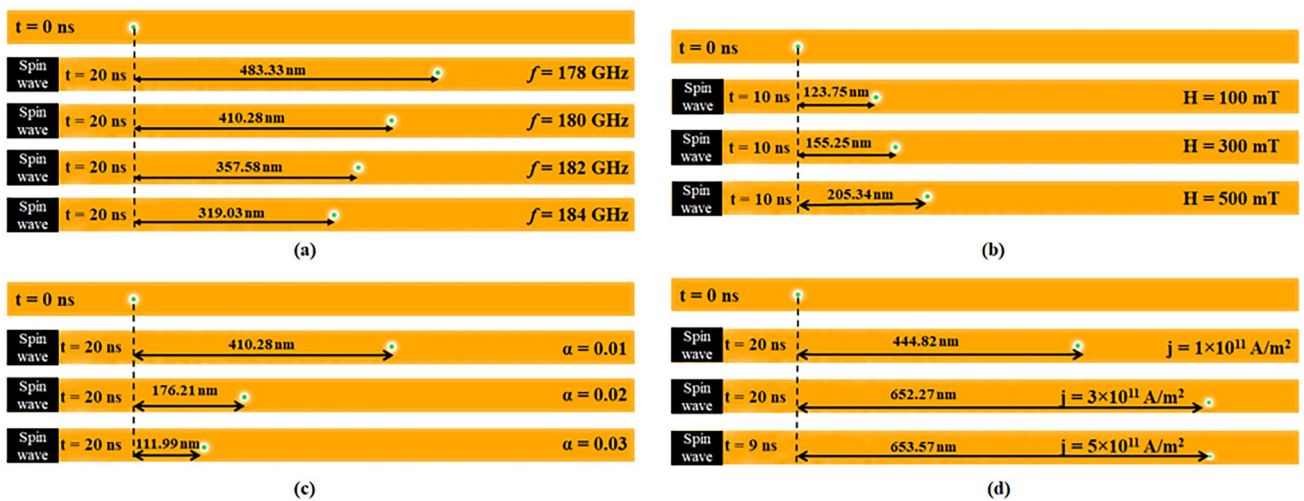

Fig. 5 Instantaneous position of the magnetic skyrmion at specific time during simulation when the following parameters are varied: **a** frequency of the spin wave, **b** amplitude of the spin wave, **c** Gilbert damping coefficient, and **d** current density strength. The position of the skyrmion is recorded by considering the top view of the z-component magnetization configuration at different times

of the skyrmion at $t = 20\,ns$ at different frequencies. The maximum velocity of the skyrmion is $29.63\,ms^{-1}$ when $f = 177\,GHz$. The value of the maximum velocity decreases with the increase in frequency of the magnetic field. The velocity of the skyrmion is inversely proportional to the applied frequency in the investigated window $f = 177 - 185\,GHz$. Supplementary movie 1 shows the trajectory of the magnetic skyrmion along the ferromagnetic nanotrack when driven with frequency of the spin waves equal to $180\,GHz$. Moreover, we have also determined the motion of the magnetic skyrmion when it is excited with spin wave frequencies equal or close to the gyration mode frequencies of the magnetic skyrmion. To find this, the entire system is excited with a sinc pulse in a $H_o = 50\,mT$ biasing field applied along the positive x-direction. The frequency response of the system is found out by performing the Fast Fourier Transform (FFT) of the z-component of magnetization. The frequency response of the magnetic skyrmion indicates that the resonance mode of the magnetic skyrmion is at $6.3744\,GHz$. When the frequency of the applied spin waves is equal to or very close to the gyration mode frequency, the trajectory of the magnetic skyrmion follows a rectilinear path in contrast to the zigzag motion which was observed for spin waves having frequencies less than or equal to $20\,GHz$. Supplementary movie 2 shows the skyrmion motion along the nanotrack with applied frequency equal to its gyration mode frequency ($f = 6.3744\,GHz$).

3.1.2 Variation of the Amplitude of the Spin Wave

Next, the amplitude of the applied spin wave is varied from $100\,mT$ to $500\,mT$ in steps of $50\,mT$. The frequency of the spin wave is kept at $180\,GHz$, and the damping coefficient is $\alpha = 0.01$ in all the cases. The skyrmion does not experience acceleration in its motion up to $200\,mT$, and it starts accelerating when the amplitude of the spin wave increases gradually. As the amplitude of the magnetic field increases, it exerts a larger torque on the skyrmion, and the velocity increases non-uniformly and reaches its maximum value. As the spin wave decays with distance, the velocity of the skyrmion decreases. Figure 3b shows the instantaneous velocities of the skyrmion at different amplitudes. The skyrmion attains maximal velocity and a larger average velocity ($v_{avg} = 20.58\,ms^{-1}$) when $H_o = 500\,mT$. When the amplitude of the field is $500\,mT$, the maximum instantaneous velocity of the skyrmion is $22.98\,ms^{-1}$ at $t = 8\,ns$. The average velocity of the skyrmion at different amplitudes as a function of time is plotted in Fig. 4b, while the position of the skyrmion at $t = 10\,ns$ at different amplitudes of the field can be seen

in Fig. 5b. Thus, a larger value of amplitude of the spin wave results in longer distances traveled by the magnetic skyrmion along the nanostrip at the same time, which reflects a higher maximum velocity and also a larger average velocity of the magnetic skyrmion. Supplementary movie 3 shows the trajectory of the magnetic skyrmion along the ferromagnetic nanotrack when driven with amplitude of the spin waves equal to $300\,mT$.

3.1.3 Variation in the Gilbert Damping Parameter

The propagation of the skyrmion along the nanotrack is recorded with different Gilbert damping parameter values. The values of the amplitude and frequency of the spin wave are $500\,mT$ and $180\,GHz$, respectively. When $\alpha = 0.01$, the skyrmion moves 410.28 nm in $t = 20\,ns$. But when the value of the damping coefficient increases to 0.02, it moves 176.21 nm in $t = 20\,ns$. However, when $\alpha = 0.03$, it moves a mere distance of 112 nm in $t = 20\,ns$, as shown in Fig. 5c. Therefore, the motion of the skyrmion is greatly reduced with the increasing damping coefficient of the system with the application of the same spin wave and spin current specifications, respectively. In addition to this, the skyrmion does not experience an acceleration in its motion as the value of the damping coefficient increases. The spin wave will be attenuated during transmission due to the increased damping of the nanostrip. Consequently, choosing materials with a lower damping constant helps to achieve skyrmion motion at high velocities that are driven by spin current and spin waves. The skyrmion velocity curve as a function of time differs from others when the damping constant is $\alpha = 0.01$. Before $36\,ns$, there is a noticeable rise in the displacement on the x-axis, and then there is a gradual decline over time. This shows that the skyrmion moves initially in the $+x$ direction and approaches the right end of the nanostrip rather closely, and since $\alpha = 1$ is set between $x = 850$ nm and 1000 nm, it encounters a repulsive force from the right end of the nanostrip, which causes its velocity to drop. Figure 3c shows the instantaneous velocities of the skyrmion at different values of the damping coefficient. Since the amplitude of the excited spin wave decays with the increase in Gilbert damping parameter values, it cannot exert the required amount of torque for the accelerated motion of the skyrmion. The average velocities of the skyrmion at different values of the Gilbert damping coefficient are shown in Fig. 4c. An inverse proportional function of the damping constant is shown in the average velocity. The maximum velocity of the skyrmion when $\alpha = 0.01$ is $22.98\,ms^{-1}$, with an average velocity of $16.64\,ms^{-1}$. Supplementary movie 4 shows the trajectory of the magnetic skyrmion along the ferromagnetic nanotrack when the Gilbert damping parameter is set at $\alpha = 0.02$.

3.1.4 Variation in Current Density of Spin-Polarized Current

The current density of the spin-polarized current is varied from $j = 1 \times 10^{11} A/m^2$ to $= 5 \times 10^{11} A/m^2$, and the motion of the skyrmion is recorded simultaneously. Figure 3d shows the instantaneous velocities of the skyrmion at different current densities as it moves along the nanostrip. The skyrmion motion shows a negligible acceleration in its motion along the nanostrip while varying the current density values. Moreover, the skyrmion shows almost zero acceleration in its motion through the nanostrip as the value of the current density increases. The instantaneous velocity of the skyrmion increases as the current density increases progressively; it rapidly approaches the right extremity of the nanostrip, reverses course, and proceeds in the opposite direction. As the skyrmion approaches the right end of the nanostrip, it encounters a repulsive force from that end, which forces it to go in the other direction and results in a reduction in displacement. When the driving power of the spin waves equalizes the repelling force of the skyrmion edge, the motion slows down and eventually stops. We compute the average velocity of the magnetic skyrmion from zero to the instant before it changes its direction of travel. Moreover, when $= 5 \times 10^{11} A/m^2$, the magnetic skyrmion becomes small in size and eventually reaches very close to the boundary of the nanotrack and stays in that position for a longer duration but does not get annihilated at the edges of the nanotrack. When the current density is low, the divergence of the magnetic skyrmion from its rectilinear path caused by the Magnus force (Skyrmion Hall Effect; SkHE) is virtually minimal. A greater degree of path deviation from the longitudinal direction is observed as the current density increases in strength. Figures 4d and 5d display the average velocity of the skyrmion at different j values and instantaneous position of the skyrmion at times indicated in the images. Supplementary movies 5 and 6 show the trajectory of the magnetic skyrmion along the ferromagnetic nanotrack when the strength of the applied current density is $j = 1.0 \times 10^{11} A/m^2$ and $j = 5.0 \times 10^{11} A/m^2$.

Thus, the above results show that the simultaneous application of spin-polarized current and the injection of spin waves into the ferromagnetic nanotrack enhances the velocity of the magnetic skyrmion far more than the application of spin waves alone [43]. Furthermore, spin-polarized current and spin-wave injection provide comprehensive control over the skyrmion's acceleration and deceleration in a magnetic nanostrip. We have also checked the motion and trajectory of the magnetic skyrmion with the injection of spin waves alone. The magnetic skyrmion exhibits a marginal greater deviation from its longitudinal trajectory when solely spin waves are employed. Moreover, a significant decrease in the magnetic skyrmion velocity is seen by only introducing spin waves into the ferromagnetic nanotrack. However, the injection of spin waves alone does not cause it to be destroyed at the ferromagnetic nanotrack boundary.

4 Conclusion

As a concluding remark, we have studied the motion of a magnetic skyrmion on a nanostrip with perpendicular magnetic anisotropy using micromagnetic simulations. The skyrmion reveals novel properties when it is confined to the nanostrip. Our study indicates that the change in magnetic moment in the nanostrip is due to the momentum exchange between spin waves and the magnetic skyrmion and the STT effect generated by the vertical spin current, causing the skyrmion to move. The acceleration and deceleration of the skyrmion in a magnetic nanostrip can be thoroughly manipulated with the use of spin-polarized current and spin-wave injection. The accelerated motion of the skyrmion can be generated with relatively low spin current densities when an external radio-frequency field is applied to inject the spin wave into the nanostrip. The decelerated motion of the skyrmion starts when the amplitude of the spin wave decays as it moves away from the region of excitation. It is found that the motion of the skyrmion is strongly dependent on parameters like the frequency of the spin wave, the amplitude of the spin wave, the Gilbert damping coefficient, and the applied spin-polarized current. The velocity is inversely related to the damping constant α and proportionate to the driving force supplied by the spin wave. These results and findings will definitely help scientists and engineers design spin waves and spin current-driven magnetic skyrmion-based devices in the future.

Declarations

Competing Interests The authors declare no competing interests.

References

1. Joo, S., Kim, T., Shin, S.H., Lim, J.Y., Hong, J., Song, J.D., Chang, J., Lee, H.-W., Rhie, K., Han, S.H., Shin, K.-H., Johnson, M.: Magnetic-field-controlled reconfigurable semiconductor logic. Nature **494**, 72 (2013). https://doi.org/10.1038/nature11817
2. Parkin, S.S.P.: (U S Patent). **6**, 834,005 (21 December 2004)
3. Parkin, S.S.P., Hayashi, M., Thomas, L.: Magnetic domain-wall racetrack memory. Science **320**, 190 (2008). https://doi.org/10.1126/science.114579
4. Parkin, S.S.P., Yang, S.-H.: Memory on the racetrack. Nat. Nanotechnol. **10**, 195 (2015). https://doi.org/10.1038/nnano.2015.41
5. Bogdanov, A.N., Yablonskii, D.A.: Thermodynamically stable vortices in magnetically ordered crystals. The mixed state of magnets. Zh. Eksp. Teor. Fiz. **95**, 178 (1989)
6. Sampaio, J., Cros, V., Rohart, S., Thiaville, A., Fert, A.: Nucleation, stability and current-induced motion of isolated magnetic skyrmions in nanostructures. Nat. Nanotechnol. **8**, 839 (2013). https://doi.org/10.1038/nnano.2013.210
7. Fert, A., Cros, V., Sampaio, J.: Skyrmions on the track. Nat. Nanotechnol. **8**, 152 (2013). https://doi.org/10.1038/nnano.2013.29
8. Skyrme, T.H.R.: A non-linear field theory. Proc. R. Soc. Lond. A Math. Phys. Eng. Sci. **260**, 127 (1961). https://doi.org/10.1098/rspa.1961.0018
9. Skyrme, T.H.R.: A unified field theory of mesons and baryons. Nuclear Phys. **31**, 556 (1962). https://doi.org/10.1016/0029-5582(62)90775-7
10. Yu, X.Z., Onose, Y., Kanazawa, N., Park, J.H., Han, J.H., Matsui, Y., Nagaosa, N., Tokura, Y.: Real-space observation of a two-dimensional skyrmion crystal. Nature **465**, 901 (2010). https://doi.org/10.1038/nature09124
11. Li, Y.F., Kanazawa, N., Yu, X.Z., Tsukazaki, A., Kawasaki, M., Ichikawa, M., Jin, X.F., Kagawa, F., Tokura, Y.: Robust formation of skyrmions and topological hall effect anomaly in epitaxial thin films of MnSi. Phys. Rev. Lett. **110**, 117202 (2013). https://doi.org/10.1103/PhysRevLett.110.117202
12. Tonomura, A., Yu, X.Z., Yanagisawa, K., Matsuda, T., Onose, Y., Kanazawa, N., Park, H.S., Tokura, Y.: Real-space observation of skyrmion lattice in helimagnet MnSi thin samples. Nano Lett. **12**, 1673 (2012). https://doi.org/10.1021/nl300073m
13. Yu, X.Z., Kanazawa, N., Onose, Y., Kimoto, K., Zhang, W.Z., Ishiwata, S., Matsui, Y., Tokura, Y.: Near room-temperature formation of a skyrmion crystal in thin-films of the helimagnet FeGe. Nat. Mater. **10**, 106 (2011). https://doi.org/10.1038/nmat2916
14. Mühlbauer, S., Binz, B., Jonietz, F., Pfleiderer, C., Rosch, A., Neubauer, A., Georgii, R., Böni, P.: Skyrmion lattice in a chiral magnet. Science **323**, 915 (2009). https://doi.org/10.1126/science.1166767
15. Münzer, W., Neubauer, A., Adams, T., Mühlbauer, S., Franz, C., Jonietz, F., Georgii, R., Böni, P., Pedersen, B., Schmidt, M., Rosch, A., Pfleiderer, C.: Skyrmion lattice in the doped semiconductor Fe$_{1-x}$Co$_x$Si. Phys. Rev. B **81**, 041203 (2010). https://doi.org/10.1103/PhysRevB.81.041203
16. Grigoriev, S.V., Chernyshov, D., Dyadkin, V.A., Dmitriev, V., Maleyev, S.V., Moskvin, E.V., Menzel, D., Schoenes, J., Eckerlebe, H.: Crystal handedness and spin helix chirality in Fe$_{1-x}$Co$_x$Si. Phys. Rev. Lett. **102**, 037204 (2009). https://doi.org/10.1103/PhysRevLett.102.037204
17. Du, H.F., DeGrave, J.P., Xue, F., Liang, D., Ning, W., Yang, J.Y., Tian, M.L., Zhang, Y.H., Jin, S.: Highly stable skyrmion state in helimagnetic MnSi nanowires. Nano Lett. **14**, 2026 (2014). https://doi.org/10.1021/nl5001899
18. Yu, X.Z., DeGrave, J.P., Hara, Y., Hara, T., Jin, S., Tokura, Y.: Observation of the magnetic skyrmion lattice in a MnSi nanowire by Lorentz TEM. Nano Lett. **13**, 3755 (2013). https://doi.org/10.1021/nl401687d
19. Moriya, T.: Anisotropic superexchange interaction and weak ferromagnetism. Phys. Rev. **120**, 91 (1960). https://doi.org/10.1103/PhysRev.120.91
20. Dzyaloshinskii, I.: A thermodynamic theory of weak ferromagnetism of antiferromagnetics. J. Phys. Chem. Solids **4**, 241 (1958). https://doi.org/10.1016/0022-3697(58)90076-3
21. Heide, M., Bihlmayer, G., Blügel, S.: Dzyaloshinskii-Moriya interaction accounting for the orientation of magnetic domains in ultrathin films: Fe/W (110). Phys. Rev. B **78**, 140403 (2008). https://doi.org/10.1103/PhysRevB.78.140403
22. Fert, A.R.: Magnetic and transport properties of metallic multilayers. Mater. Sci. Forum. **59–60**, 439–480 (1991). https://doi.org/10.4028/www.scientific.net/MSF.59-60.439
23. Fert, A., Levy, P.M.: Role of anisotropic exchange interactions in determining the properties of spin-glasses. Phys. Rev. Lett. **44**, 1538 (1980). https://doi.org/10.1103/PhysRevLett.44.1538
24. Ran, N., Zhao, G.P., Tang, H., Shen, L.C., Lai, P., Xia, J., Zhang, X., Zhou, Y.: The influence of the edge effect on the skyrmion generation in a magnetic nanotrack. AIP Adv. **7**, 025105 (2017). https://doi.org/10.1063/1.4976726
25. Zhang, X., Zhou, Y., Ezawa, M., Zhao, G.P., Zhao, W.: Magnetic skyrmion transistor: skyrmion motion in a voltage-gated nanotrack. Sci. Rep. **5**, 11369 (2015). https://doi.org/10.1038/srep11369
26. Zhang, X., Zhou, Y., Ezawa, M.: Magnetic bilayer-skyrmions without Skyrmion Hall effect. Nat. Commun. **7**, 10293 (2016). https://doi.org/10.1038/ncomms10293
27. Tomasello, R., Martinez, E., Zivieri, R., Torres, L., Carpentieri, M., Finocchio, G.: A strategy for the design of skyrmion racetrack memories. Sci. Rep. **4**, 6784 (2014). https://doi.org/10.1038/srep06784
28. Zhang, X., Ezawa, M., Zhou, Y.: Magnetic skyrmion logic gates: conversion, duplication and merging of skyrmions. Sci. Rep. **5**, 9400 (2015). https://doi.org/10.1038/srep09400
29. Tchoe, Y., Han, J.H.: Skyrmion generation by current. Phys. Rev. B **85**, 174416 (2012)
30. Del-Valle, N., Agramunt-Puig, S., Sanchez, A., Navau, C.: Imprinting skyrmions in thin films by ferromagnetic and superconducting templates. Appl. Phys. Lett. **107**, 133103 (2015). https://doi.org/10.1063/1.4932090
31. Koshibae, W., Kaneko, Y., Iwasaki, J., Kawasaki, M., Tokura, Y., Nagaosa, N.: Memory functions of magnetic skyrmions. Jpn. J. Appl. Phys. **54**, 053001 (2015). https://doi.org/10.7567/JJAP.54.053001
32. Romming, N., Hanneken, C., Menzel, M., Bickel, J.E., Wolter, B., von Bergmann, K., Kubetzka, A., Wiesendanger, R.: Writing and deleting single magnetic skyrmions. Science **341**, 636 (2013). https://doi.org/10.1126/science.1240573
33. Iwasaki, J., Mochizuki, M., Nagaosa, N.: Universal current-velocity relation of skyrmion motion in chiral magnets. Nat. Commun. **4**, 1463 (2013). https://doi.org/10.1038/ncomms2442
34. Iwasaki, J., Beekman, A.J., Nagaosa, N.: Theory of magnon-skyrmion scattering in chiral magnets. Phys. Rev. B **89**, 064412 (2014). https://doi.org/10.1103/PhysRevB.89.064412
35. Lin, S.Z., Reichhardt, C., Batista, C.D., Saxena, A.: Driven skyrmions and dynamical transitions in chiral magnets. Phys. Rev. Lett. **110**, 207202 (2013). https://doi.org/10.1103/PhysRevLett.110.207202
36. Donahue, M., Porter, D.G., User's, O.O.M.M.F.: Guide, version1.0 National Institute of Standard and Technology, Gaithersburg, MD, Interagency Report NISTIR 6376 [Online] (1999). Available: http://math.nist.gov/oommf

37. Brown, W.F. Jr.: Domains, micromagnetics, and beyond: reminiscences and assessments. J. Appl. Phys. **49**, 1937 (1978). https://doi.org/10.1063/1.324811

38. Landau, L., Lifshitz, E.: On the theory of the dispersion of magnetic permeability in ferromagnetic bodies. Physik Z. Sowjetunion **8**, 153 (1935). https://doi.org/10.1016/B978-0-08-036364-6.50008-9

39. Gilbert, T.L.: Phys. Rev 100, 1243 ; A phenomenological theory of damping in ferromagnetic materials. IEEE Trans. Magn. **40**, 3443 (2004). (1955). https://doi.org/10.1109/TMAG.2004.836740

40. Xiao, J., Zangwill, A., Stiles, M.D.: Boltzmann test of Slonczewski's theory of spin-transfer torque. Phys. Rev. B **70**, 172405 (2004). https://doi.org/10.1103/PhysRevB.70.172405

41. Thiaville, A., Rohart, S., Jué, É., Cros, V., Fert, A.: Dynamics of Dzyaloshinskii domain walls in ultrathin magnetic films. Europhys. Lett. **100**, 57002 (2012). https://doi.org/10.1209/0295-5075/100/57002

42. Schroeter, S., Garst, M.: Scattering of high-energy magnons off a magnetic skyrmion. Low Temp. Phys. **41**, 817 (2015). https://doi.org/10.1063/1.4932356

43. Zhang, G., Tian, Y., Deng, Y., Jiang, D., Deng, S.: Spin-wave-driven skyrmion motion in magnetic nanostrip, J. Nanotechnol. **2018**, 2602913 (2018). https://doi.org/10.1155/2018/2602913